Submitted to

Europhysics Conference on High Energy Physics, EPS2007, July 19-25, 2007, Manchester
Abstract: **173**
Parallel Session **Strong Interactions**

Electronic Access: www-h1.desy.de/h1/www/publications/conf/conf_list.html

$\mathrm{D}^{\star}$-Meson Production in Deep Inelastic Scattering at HERA

H1 Collaboration

Abstract

Inclusive production of $D^{\star}$ mesons in deep inelastic scattering at HERA is studied. The data were taken with the H1 detector in the years 2004 to 2006 and correspond to an integrated luminosity of 222 pb^{-1} thus increasing the available data by a factor 5 compared to the previous publication. This analysis covers the region $5 < Q^2 < 100$ GeV^2 in the photon virtuality and $0.05 < y < 0.6$ in the inelasticity of the scattering process. The visible range for the $D^{\star}$ meson is $p_t(D^{\star}) > 1.5$ GeV and $|\eta(D^{\star})| < 1.5$. Single and double differential cross sections are compared to predictions from the next-to-leading order calculation HVQDIS and the leading order simulation programs RAPGAP and CASCADE.

1 Introduction

At HERA in deep inelastic electron proton scattering heavy quarks are predominantly produced in the boson gluon fusion process (figure 1) and their study thus offers a direct sensitivity to the gluon density in the proton. Here the virtual photon from the electron interacts with a gluon from the proton via the production of a charm anti-charm quark pair. The high mass of charm quarks of about 1.5 GeV provides at least one hard scale for perturbative QCD (pQCD) predictions in the whole phase space. These calculations are complicated due to the presence of additional hard scales like the virtuality of the exchanged photon Q^2 and the transverse momentum of the charm quark p_t. The increased statistics of the new HERA II data compared to the previous analysis [1] makes more detailed tests of pQCD predictions at LO and NLO possible.

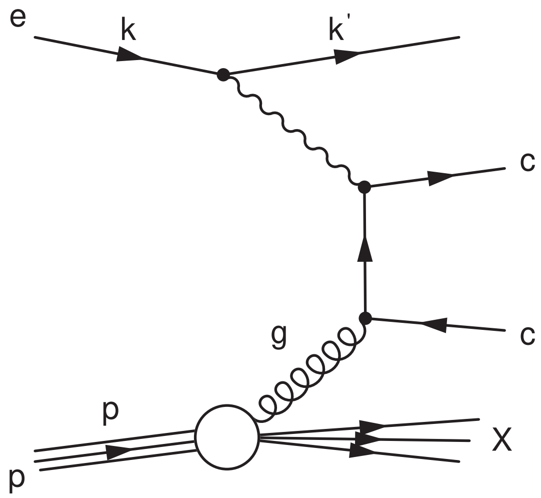

Figure 1: Feynman Graph for boson gluon fusion in leading order α_s

2 H1 Detector

The H1 detector is described in detail in [2, 3]. Here only the detector components relevant for this analysis are shortly described.

Charged particles emerging from the ep interaction region are measured within the central tracking detector (CTD) in the rapidity range $-1.74 < \eta < 1.74$. The CTD consists of two large cylindrical jet chambers (CJC1 & 2), which are separated by a z-chamber (COZ). These chambers are arranged concentrically around the interaction region in a magnetic field of 1.16 T. On the first three trigger levels the fast track trigger (FTT [4]) provides trigger information based on reconstructed tracks from the CJC1 & 2.

Charged and neutral particles are measured in the liquid argon (LAr) calorimeter, which surrounds the tracking chambers and covers the range $-1.5 < \eta < 3.4$, and in a lead–scintillating fibre calorimeter (SpaCal) covering the backward region $-4.0 < \eta < -1.4$. The SpaCal is used for identification of deep inelastic scattering events. The measurements of the CTD and both calorimeters are combined to reconstruct the final state particles.

The luminosity determination is based on the measurement of the Bethe-Heitler process ($ep \rightarrow ep\gamma$) where the photon is detected in a calorimeter located downstream of the interaction region in the electron direction.

3 Event Selection

The data sample corresponds to an integrated luminosity of 222 pb^{-1} and was recorded with the H1 experiment in the years 2004–2006, where either electrons or positrons at 27.6 GeV were collided with protons at 920 GeV. The events are triggered by a high, local energy deposit in the SpaCal in coincidence with a least one track with a transverse momentum greater that 0.9 GeV reconstructed by the FTT.

DIS events are selected by requiring an isolated high energy electromagnetic cluster in the SpaCal which is consistent with the scattered electron. The reconstruction of the negative four momentum transfer squared from the electron to the proton (photon virtuality) is based only on the measurement of the scattered electron using the so called electron method. Here the photon virtuality Q^2 is calculated from the energy of the incoming and outgoing electron E_e and E'_e, respectively, and the scattering angle θ_e of the scattered electron: $Q^2 = E_e E'_e\,(1 + \cos\theta_e)$. The inelasticity y (the energy fraction transferred from the lepton to the hadronic final state in the proton rest frame) is given by: $y = 1 - \frac{E'_e}{2E_e}(1 - \cos\theta_e)$. Bjorken x, the fractional momentum of the parton to the momentum of the proton, is also reconstructed based solely on the SpaCal measurement: $x = \frac{Q^2}{y \cdot s}$, where $\sqrt{s}$ is the centre of mass energy. The visible kinematical region for the photon virtuality is restricted to $5 < Q^2 < 100$ GeV^2 and for the inelasticity to values of $0.05 < y < 0.6$.

Events, in which charm quarks have been produced, are identified by reconstructing $D^\star$ mesons decaying in their golden decay channel:

$$D^{\star\pm} \rightarrow D^0 \pi^\pm_{\text{slow}} \rightarrow K^\mp \pi^\pm \pi^\pm_{\text{slow}}. \tag{1}$$

In order to calculate the total production cross section of the $D^\star$ mesons, the branching fraction of the golden decay of 2.35% is used [5]. Due to the small difference in the invariant masses of the $D^\star$ and D^0 mesons the slow pion, π_{slow}, is produced with a small transverse momentum p_t.

The tracks of the decay particles are reconstructed by the CTD and are therefore restricted to a polar angle of $20^\circ < \theta < 160^\circ$. The kaon and the pion are required to have a transverse momentum greater than 0.3 GeV and the slow pion above 0.12 GeV. A cut on the scalar sum of transverse momentum of the pion and kaon above 2.0 GeV is made in order to suppress background from the light quarks u,d and s. Due to these cuts the visible region, in which $D^\star$ mesons are reconstructed, is restricted to $p_t(D^\star) > 1.5$ GeV and to the pseudo-rapidity[1] of $|\eta| < 1.5$.

[1]The pseudo-rapidity is given by $\eta = -\ln\tan(\theta/2)$ where θ is measured with respect to the the z-axis given by the proton beam.

The two subsequent decays can be used to calculate the variable

$$\Delta M = M(K\pi\pi_{\mathrm{slow}}) - M(K\pi), \tag{2}$$

where $M(K\pi\pi_{\mathrm{slow}})$ and $M(K\pi)$ are the invariant masses of the three and two body decays, respectively. The distribution of the $K\pi$-mass and ΔM are shown in figure 2. The so called wrong charge (WC) background is selected similarly: the kaon and pion have the same charge, such that these particles cannot origin from a D meson. The π_{slow} must have the opposite charge. Since the shape of the WC background is determined by combinatorics it can be used to constrain the shape of the background especially in the signal region.

The number of $D^\star$ mesons is determined by a fit to the ΔM distribution. As the signal has a tail towards larger ΔM an asymmetric probability density function [6][2] is chosen:

$$f_{CB}(m) = N \cdot \begin{cases} \exp\left(-\frac{1}{2}\left(\frac{m-\mu}{\sigma}\right)\right)^2 & \text{if } \frac{m-\mu}{\sigma} \leq \alpha \\ \frac{\left(\frac{n}{|\alpha|}\right)^n \exp\left(-\frac{1}{2}\alpha^2\right)}{\left(\frac{n}{|\alpha|}-|\alpha|-\frac{m-\mu}{\sigma}\right)^n} & \text{if } \frac{m-\mu}{\sigma} > \alpha. \end{cases} \tag{3}$$

This distribution consists of a Gaussian function where on one side a power law is attached such that the resulting function remains steady. Here N is the normalisation of the function, μ is the most probable value and σ the width of the distribution. The variables n and α describe the form of the tail which is chosen to be on the right side here.

In order to describe the shape of the background the Granet parametrisation [7] is used:

$$f_{Gr}(m) = p_0 \cdot (m - m_\pi)^{p_1} \cdot \exp(-p_2 m) \tag{4}$$

Here p_0 is the normalisation while p_1 and p_2 determine the shape of the distribution.

The sum of these two functions is fitted to the data using an unbinned log likelihood fit simultaneous to the signal data set and the WC background distribution. An additional term in the likelihood function is added, such that the integral of the function is identical to the sum of the entries in the corresponding data distribution. This fit is performed using the rooFit framework [8].

During the fit the contributions from reflections to the signal are taken into account. This contribution is deduced using a dedicated Monte-Carlo simulation of pure charm events and is found to amount to 4%. The fit to the complete data set yields $N(D^\star) = 10333 \pm 233$ thus increasing the amount of reconstructed $D^\star$-mesons by a factor of four compared to the previous analysis [1] even so the kinematical region of the present analysis is smaller. For each analysis bin a fit to the ΔM spectrum is performed, but in order to improve the convergence at lower statistics the parameters n and α are fixed to the value of the fit to the complete data set. The width of the peak can vary in dependence of the event kinematics and is therefore left free.

The MC program RAPGAP 3.1 [9] is used to correct the data for detector acceptance and efficiencies and is also used for comparison to the data. It implements the DGLAP evolution

[2] This function was first used by the Crystal Ball Collaboration to describe the radiative tail in $J/\psi \to e^+e^-$.

equation and uses CTEQ6L [10] as proton PDF. The renormalization scale is set to $\mu_r^2 = Q^2$. The RAPGAP event generator is interfaced to a detailed simulation of the H1 detector based on GEANT [11]. A good description of the data by this simulation is achieved [12].

The data are also compared to LO predictions from the Monte-Carlo program CASCADE 1.2 [13] and NLO predictions from the program HVQDIS [14, 15]. CASCADE implements k_t-factorization and is based on the CCFM evolution. It uses J2003 set 3 [16] for the gluon-density in the proton and the renormalization scale is set to $\mu_r^2 = 4m_q^2 + p_t^2$. Both MC programs use the Lund string model for the hadronization of light quarks. Heavy quarks are fragmented according to the Bowler function with the parameter settings $a = 0.437$ and $b = 0.850$. HVQDIS implements the Fixed Flavour Numbering Scheme (FFNS) for the treatment of heavy quarks. Renormalization and factorization scale are set to $\mu_r^2 = \mu_f^2 = 4m_c^2 + Q^2$. The central value for the charm mass is set to 1.45 GeV with a variation between 1.3 and 1.6 GeV. For the proton CTEQ5F3 [17] is used as PDF. The charm quarks are fragmented according to the Peterson function into $D^\star$ mesons using the value $\epsilon_c = 0.045$. The range of the charm mass and the value of the Peterson fragmentation parameter are chosen to describe the data.

4 Systematic Uncertainties

The dominating systematic uncertainties of this measurement are shortly discussed here, more details can be found in [12].

The systematic error on the track efficiency of 7% per $D^\star$ meson is the dominant error of this measurement. It is split into three contributions: (i) The difference in the track finding efficiency between data and simulations is analysed using as a reference electrons detected in the LAr calorimeter leading to an error of 2% per track. (ii) The efficiency with which a track can be fit to the event vertex leads to a systematic error of 2.5% per $D^\star$ meson. (iii) The track efficiency also depends on the nuclear interaction probability of the decay particles in the detector material. This gives rise to a systematic error of 2.5% per $D^\star$ meson.

Using a different parameterisation for signal and background shape the systematic uncertainty on the signal extraction is estimated to be 2%. This reduces this error significantly compared to the previous measurement [1] where a symmetric probability density function has been used for the signal.

The contribution to the signal caused by reflections is studied as a function of p_t and found to vary within $\pm 3.5\%$ which is taken into account in the systematic error.

The systematic uncertainty on the SpaCal energy calibration is measured to be about 1%. The influence is studied individually for each analysis bin. It results usually in a systematic error of the order of 1 to 2.5%, but due to migrations it leads to deviations of up to 35% and 13% in the regions of large $z_{D^\star}$ [3] and $\eta_{D^\star}$, respectively.

All sources of the systematic errors are assumed to be uncorrelated and are added in quadrature. On average this results in a systematic error of about 8.5%, and the measurement is therefore systematically dominated in most regions of the kinematic phase space.

[3]The inelasticity of the of the $D^\star$ meson $z_{D^\star}$ measures the fraction of the photon energy in the proton rest frame, which is transferred to the $D^\star$ meson: $z_{D^\star} = \frac{(E-p_z)_{D^\star}}{2yE_e}$. Here $(E - p_z)_{D^\star}$ is the difference of the energy and the momentum in z direction of the $D^\star$ meson. The inelasticity $z_{D^\star}$ is closely correlated to the fragmentation variable z which is not directly accessible.

5 Results

The total visible cross section is measured to be

$$\sigma_{\rm vis}^{\rm tot}(e^{\pm}p \to e^{\pm}D^{\star\pm}X) = 4.23 \pm 0.09\ (\text{stat.}) \pm 0.37\ (\text{syst.})\ \text{nb} \tag{5}$$

in the visible region of the photon virtuality $5 < Q^2 < 100$ GeV^2, of the inelasticity $0.05 < y < 0.6$, of the transverse momentum of the $D^\star$ meson $p_t > 1.5$ GeV and of the pseudorapidity $|\eta| < 1.5$.

For the same visible region the NLO calculation HVQDIS yields $\sigma_{\rm vis}^{\rm tot} = 4.28(3.46)$ nb for a charm mass of $1.3(1.6)$ GeV, which is in good agreement with the measurement. The Monte-Carlo generator RAPGAP yields a cross section of $\sigma_{\rm vis}^{\rm tot} = 4.40$ nb and CASCADE gives $\sigma_{\rm vis}^{\rm tot} = 4.29$ nb. In both cases a charm mass of 1.5 GeV is used.

In the figures 3, 4 and 5 the single differential cross sections are shown as function of the photon virtuality Q^2, the Bjorken x and the centre of mass energy W in the γp frame respectively. The measurements are compared to the Monte-Carlo predictions by RAPGAP (dotted blue line) and CASCADE (solid red line). The prediction of the next-to-leading order calculation with the HVQDIS program is shown as the yellow band. All these predictions are able to describe the measurement well within the given uncertainties for all these distributions. The comparison with HVQDIS shows a preference for the upper edge of the prediction. The variation of the charm mass has the largest influence on the normalization of the HVQDIS prediction, meaning a small charm mass is preferred by the data.

The single differential cross sections as a function of the kinematics of the $D^\star$ meson are given in the figures 6, 7 and 8. In figure 6 it seems that the HVQDIS prediction in dependence of the transverse momentum of the $D^\star$ meson is slightly too flat, while the Monte-Carlo programs are able to describe the data properly. The HVQDIS prediction is also not able to describe the data as a function of the pseudorapidity η for $\eta > 0.5$ (figure 7), while CASCADE agrees with the data and RAPGAP is too high for $\eta < -1$. For the cross section as a function of the inelasticity $z_{D^\star}$ of the $D^\star$ meson (figure 8) HVQDIS is clearly not able to describe the shape properly. On the other hand both Monte-Carlo predictions are able to describe the inelasticity $z_{D^\star}$ reasonably well.

In order to investigate the disagreement in the pseudorapidity $\eta_{D^\star}$ between data and the HVQDIS calculation further, a double differential measurement in $p_t(D^\star)$ and $\eta_{D^\star}$ is performed. In figure 9 the cross section is presented as a function of the pseudorapidity $\eta_{D^\star}$ in bins of the transverse momentum of the $D^\star$ meson $p_t(D^\star)$. The discrepancy between the data and the HVQDIS calculation for $\eta > 0.5$ in forward direction is located solely at low transverse momenta between 1.5 GeV and 2.5 GeV. In addition there also seems to be a small discrepancy between the data and the CASCADE prediction in the most forward η bin for transverse momenta higher than 2.5 GeV, where the prediction is slightly higher than the data.

6 Conclusion

A measurement of $D^\star$ meson production in deep inelastic scattering is performed with 4-fold increased statistics in comparison to previous H1 measurements. The overall features of the data in terms of the inclusive cross section and differential cross section distributions are found to be well described by all predictions, i.e. by the leading order Monte-Carlo simulations RAPGAP and CASCADE as well as by the next-to-leading order calculation HVQDIS. In detail, however, some deviations are found between the data and the NLO prediction, especially in the forward direction, and in particular for low transverse momenta of the $D^{\star}$ meson.

Acknowledgements

We are grateful to the HERA machine group whose outstanding efforts have made this experiment possible. We thank the engineers and technicians for their work in constructing and maintaining the H1 detector, our funding agencies for financial support, the DESY technical staff for continual assistance and the DESY directorate for support and for the hospitality which they extend to the non DESY members of the collaboration.

References

[1] A. Aktas *et al.*, [H1 Coll.], Submitted to Eur.Phys.J.C, hep-ex/0701023.

[2] I. Abt *et al.*, [H1 Coll.], Nucl. Instrum. Meth. **A386** (1997) 310.

[3] I. Abt *et al.*, [H1 Coll.], Nucl. Instrum. Meth. **A386** (1997) 348.

[4] A. Schöning, [H1 Coll.], Nucl. Instrum. Meth. **A518** (2004) 542.

[5] W. M. Yao *et al.*, [Particle Data Group], J. Phys. **G33** (2006) 1.

[6] J. E. Gaiser, *Charmonium Spectroscopy from radiative Decays of the J/Ψ and Ψ'*, PhD thesis, Stanford University, 1982.

[7] P. Granet *et al.*, [French-Soviet Coll.], Nucl. Phys. **B140** (1978) 389.

[8] W. Verkerke and D. Kirkby, *The RooFit toolkit for data modeling*, PhysStat 05, 2005.

[9] J. Bartels, H. Jung, and A. Kyrieleis, hep-ph/0010300.

[10] J. Pumplin *et al.*, JHEP **07** (2002) 012, hep-ph/0201195.

[11] R. Brun *et al.*, Technical Report CERN-DD/EE-81-1 (1987).

[12] M.-O. Bönig, *Messung des $D^{\star}$-Meson-Produktionsquerschnitts in tiefinelastischer Streuung mit dem H1-Experiment*, PhD thesis, Universität Dortmund, 2007.

[13] H. Jung, *CCFM prediction on forward jets and F2: Parton level predictions and a new hadron level Monte Carlo generator CASCADE*, hep-ph/9908497.

[14] B. W. Harris and J. Smith, Nucl. Phys. **B452** (1995) 109, hep-ph/9503484.

[15] B. W. Harris and J. Smith, Phys. Rev. **D57** (1998) 2806, hep-ph/9706334.

[16] M. Hansson and H. Jung, *Status of CCFM: Un-integrated gluon densities*, hep-ph/0309009.

[17] H. L. Lai *et al.*, [CTEQ Coll.], Eur. Phys. J. **C12** (2000) 375, hep-ph/9903282.

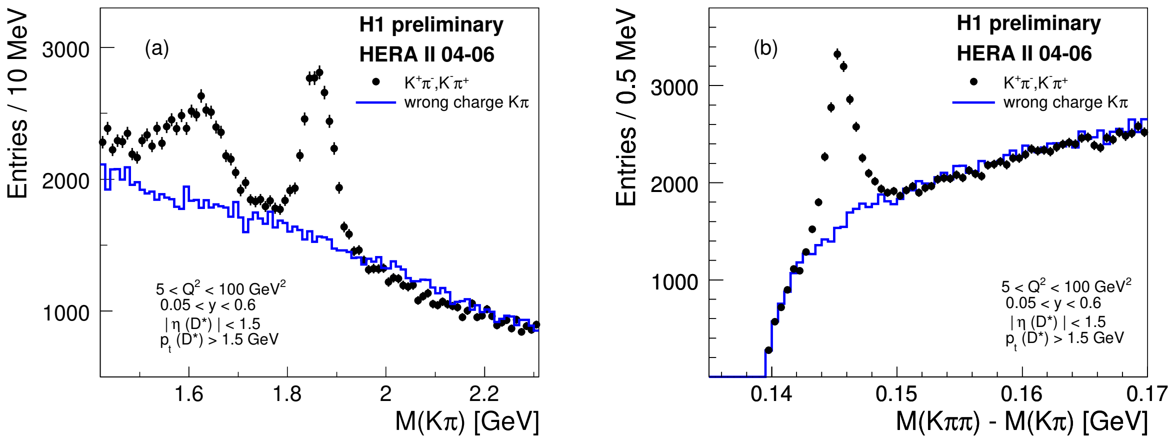

Figure 2: The invariant $K\pi$ mass distribution (a) and the distribution of $\Delta M = M(K\pi\pi_{\text{slow}}) - M(K\pi)$(b). The signal data sample is shown as black points and the wrong charged background as solid line. In both distribution a large signal of $D^\star$ mesons is visible. In (a) at low masses the reflection S_0 is present.

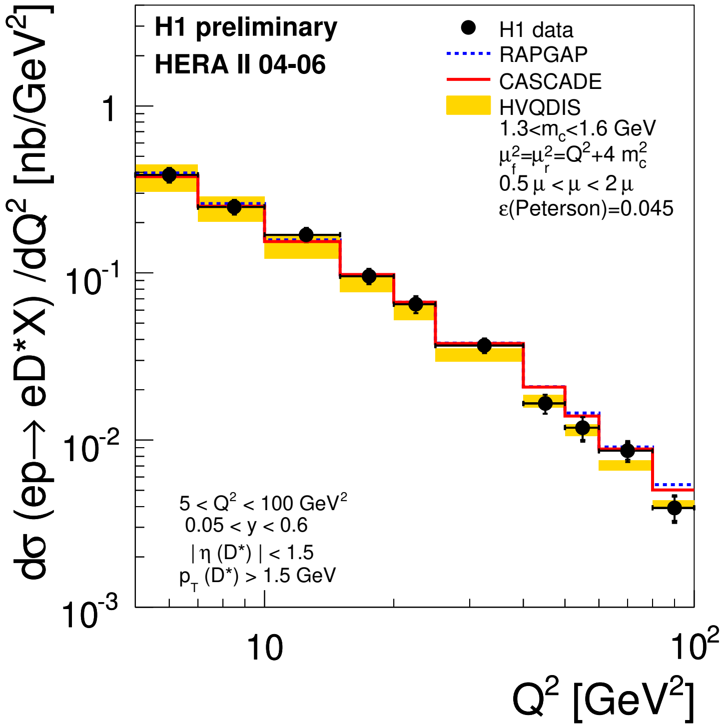

Figure 3: Differential cross section as a function of Q^2 in the visible kinematical range of $0.05 < y < 0.6$, $p_t(D^\star) > 1.5$ GeV and $|\eta(D^\star)| < 1.5$. The measurements are given as black points; the inner error bars correspond to the statistical error of the measurement, while the outer error bars correspond to the statistical and systematic error added in quadrature. For comparison LO Monte-Carlo predictions from RAPGAP (dotted line) and CASCADE (solid line) are shown. The band for the expectation of HVQDIS is obtained by varying the charm mass between 1.3 and 1.6 GeV and the renormalization and factorization scale by a factor 2 up and down.

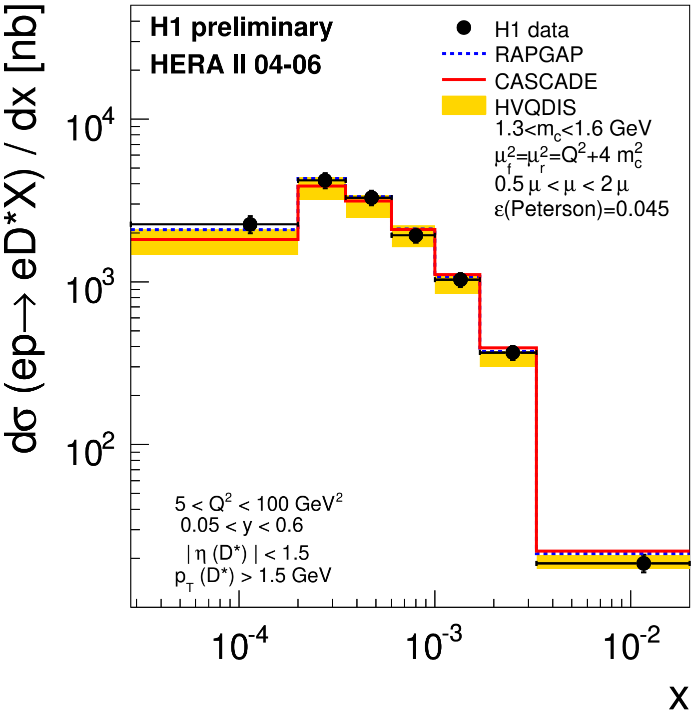

Figure 4: Differential cross section as a function of Bjorken x in the visible kinematical range of $5 < Q^2 < 100$ GeV^2, $0.05 < y < 0.6$, $p_t(D^\star) > 1.5$ GeV and $|\eta(D^\star)| < 1.5$. See the caption of figure 3 for further details.

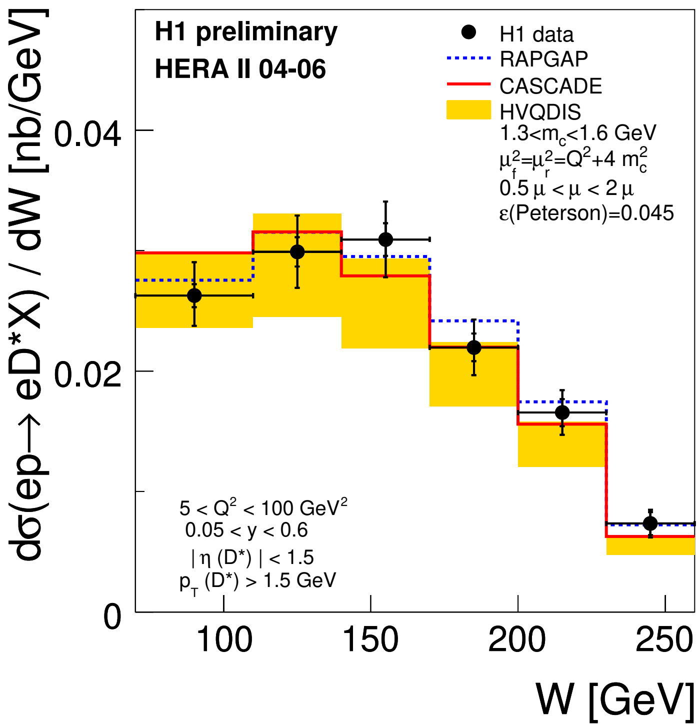

Figure 5: Differential cross section as a function of centre of mass energy W in the γp frame in the visible kinematical range of $5 < Q^2 < 100$ GeV^2, $0.05 < y < 0.6$, $p_t(D^\star) > 1.5$ GeV and $|\eta(D^\star)| < 1.5$. See the caption of figure 3 for further details.

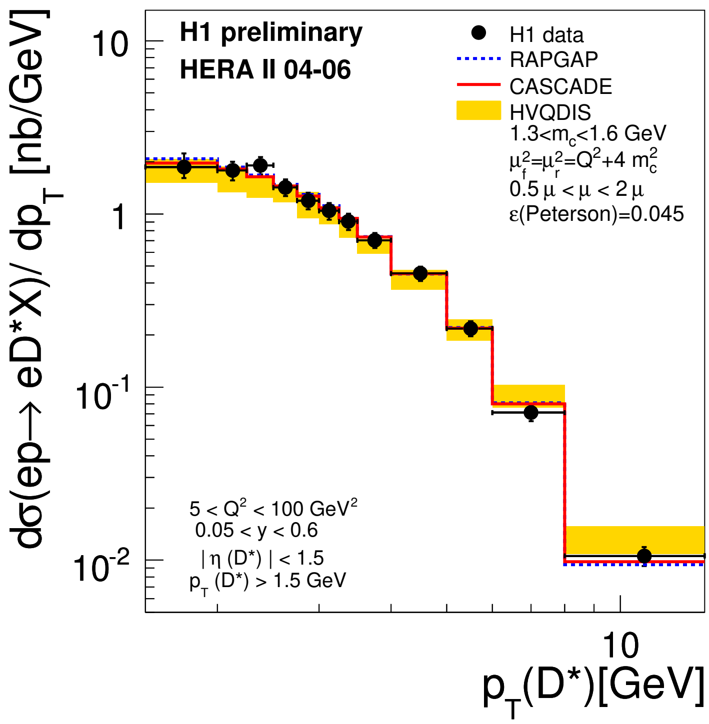

Figure 6: Differential cross section as a function of the transverse momentum of the $D^{\star}$-meson in the visible kinematical range of $5 < Q^2 < 100$ GeV^2, $0.05 < y < 0.6$ and $|\eta(D^{\star})| < 1.5$. See the caption of figure 3 for further details.

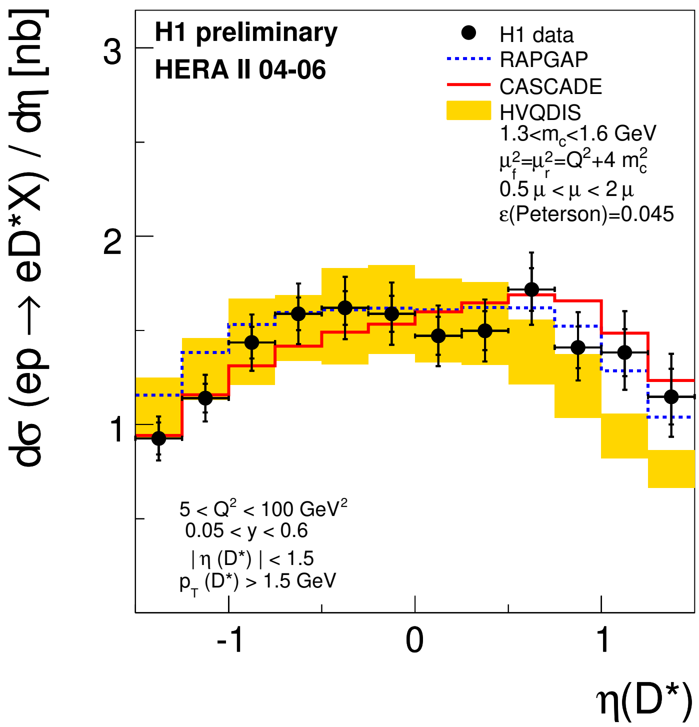

Figure 7: Differential cross section as a function of the pseudorapidity η of the $D^{\star}$-meson in the visible kinematical range of $5 < Q^2 < 100$ GeV^2, $0.05 < y < 0.6$ and $p_t(D^{\star}) > 1.5$ GeV. See the caption of figure 3 for further details.

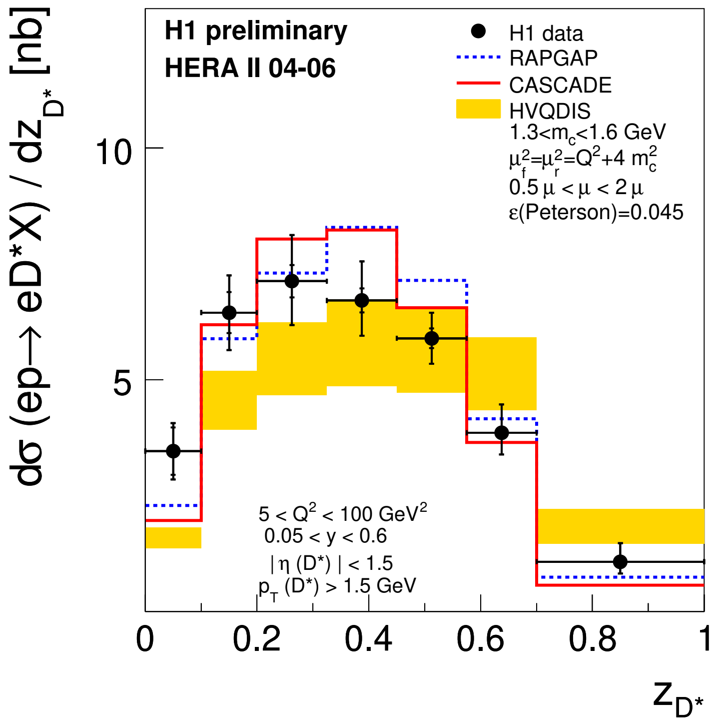

Figure 8: Differential cross sections as a function the inelasticity of the of the $D^{\star}$ meson $z_{D^{\star}}$ in the visible kinematical range of $5 < Q^2 < 100$ GeV^2, $0.05 < y < 0.6$, $p_t(D^{\star}) > 1.5$ GeV and $|\eta(D^{\star})| < 1.5$. See the caption of figure 3 for further details.

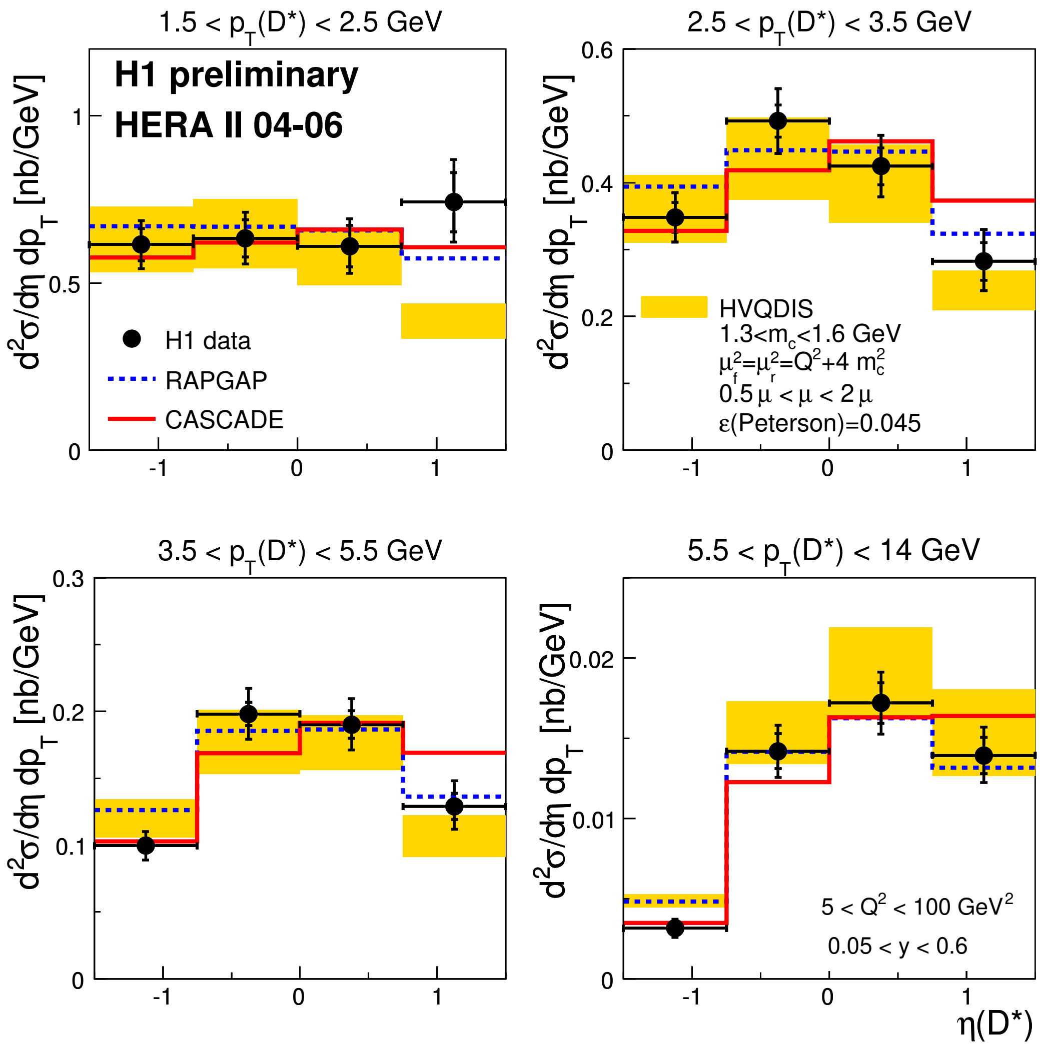

Figure 9: Double differential cross section as a function of $p_t(D^\star)$ and $\eta_{D^\star}$ in the visible kinematical range of $5 < Q^2 < 100$ GeV^2, $0.05 < y < 0.6$. See the caption of figure 3 for further details.